

# 30 GHz flux density measurements of the Caltech-Jodrell flat-spectrum sources with OCRA-p (Research Note)

S. R. Lowe<sup>1</sup>, M. P. Gawroński<sup>2</sup>, P. N. Wilkinson<sup>1</sup>, A. J. Kus<sup>2</sup>, I. W. A. Browne<sup>1</sup>, E. Pazderski<sup>2</sup>, R. Feiler<sup>2</sup>, and D. Kettle<sup>1</sup>

<sup>1</sup> University of Manchester, Jodrell Bank Observatory, Macclesfield, Cheshire, SK11 9DL, UK  
e-mail: Stuart.Lowe@manchester.ac.uk

<sup>2</sup> Toruń Centre for Astronomy, Nicolaus Copernicus University, 87-148 Toruń/Piwnice, Poland

Received June 7, 2007; accepted ???

## ABSTRACT

**Aims.** To measure the 30-GHz flux densities of the 293 sources in the Caltech-Jodrell Bank flat-spectrum (CJF) sample. The measurements are part of an ongoing programme to measure the spectral energy distributions of flat spectrum radio sources and to correlate them with the milliarcsecond structures from VLBI and other measured astrophysical properties.

**Methods.** The 30-GHz data were obtained with a twin-beam differencing radiometer system mounted on the Toruń 32-m telescope. The system has an angular resolution of 1.2'.

**Results.** Together with radio spectral data obtained from the literature, the 30-GHz data have enabled us to identify 42 of the CJF sources as Giga-hertz Peaked Spectrum (GPS) sources. Seventeen percent of the sources have rising spectra ( $\alpha > 0$ ) between 5 and 30 GHz.

**Key words.** Astronomical data bases: miscellaneous – Radio continuum: galaxies

## 1. Introduction

The emission from most flat-spectrum radio sources, from radio frequencies through gamma-rays, is thought to arise in relativistic jets and be beamed synchrotron self-Compton emission. Often described as blazar emission it is characterized by two peaks in the spectral energy distribution (SED), one synchrotron and one inverse Compton. From object to object the peak frequency can occur anywhere between  $10^{10}$  Hz to  $10^{15}$  Hz. There are claims that where the peaks occur depends systematically on radio luminosity (Fossati et al. 1998; Ghisellini et al. 2002). The correlation is in the sense that the synchrotron peak frequency increases as the luminosity decreases. This is potentially an important result but has been questioned by several authors (e.g. Antón & Browne 2005). A major problem is, however, the lack of good quality SEDs on well-defined samples of objects and for this reason we have embarked on a programme to try to rectify this deficiency. Flux density measurements at centimeter wavelengths and shorter are the most important in order to define the position of the synchrotron peak. Here we report measurements with a new receiver, OCRA-p on the Toruń 32m Telescope at a wavelength of 1cm.

The CJF sample is currently the best studied sample of flat-spectrum radio sources. The CJF sample (Taylor et al. 1996) consists of 293 sources selected from three previous VLBI surveys: the PR survey (Pearson & Readhead 1988), the first Caltech-Jodrell (CJ) survey (CJ1: Polatidis et al. 1995) and the second Caltech-Jodrell survey (CJ2: Taylor et al. 1994). The selection criteria were:

1.  $S_{4.85 \text{ GHz}} \geq 350 \text{ mJy}$
2.  $a_{1.4 \text{ GHz}}^{4.85 \text{ GHz}} \geq -0.5^1$
3.  $\delta(1950) \geq 35^\circ$
4.  $|b| \geq 10^\circ$

In addition to the structural information obtained in the CJ VLBI surveys, extensive follow-up observations have been made with the VLBA (Britzen et al. in prep) to study the statistics of superluminal motions; redshift information is available for  $> 90\%$  of the sample. Furthermore, all 293 sources have been observed in soft X-rays, either as part of the *ROSAT* All-Sky Survey or in *ROSAT* pointed observations (Britzen et al. 2002). The CJF sample is therefore a natural starting point for a programme aimed at understanding the relationships between the broadband SEDs and the spatial structure, kinematics and X-ray properties of compact radio sources. Several different types of objects are found in samples selected, like CJF, from radio surveys made at relatively low (few GHz) frequencies. While the sample is dominated by highly-relativistic “core-jet” sources it also contains the precursors of large-scale double sources (the Compact Symmetric Objects, CSOs: e.g. Wilkinson et al. 1994; Readhead et al. 1996a,b) and perhaps a few ULIRGS (typically more distant and luminous versions of the starburst galaxy, Arp 220). VLBI observations immediately distinguish between these different types: the core-jet sources are highly asymmetric, in contrast to the CSOs, while ULIRGS are highly resolved.

The complementary radio spectral information is available from hundreds of MHz to typically  $\sim 10$  GHz but information

**Table 1.** Nominal system specifications for OCRA-p on the Toruń 32-m telescope.

Frequency Range	27 – 33 GHz
System Temperature, $T_{\text{sys}}$	40 K
Individual beam FWHM	1.2'
Beam spacing	3.1'
Aperture Efficiency	45%

at higher frequencies is sparse. As part of the commissioning programme for the new One Centimetre Radio Array prototype (OCRA-p) we have measured the flux densities of all the CJF sources at 30 GHz using the Toruń 32-m Telescope. In addition to their intrinsic astrophysical interest the CJF sources are relatively strong and hence provide a first test of the OCRA-p system. Other early results with the OCRA-p system are presented elsewhere (Lancaster et al. 2007).

In sections 2 and 3 we briefly describe the OCRA-p system and the observing techniques we used to take the 30-GHz data. In section 4 we present the results in the form of a Table of 30-GHz flux densities. In section 5 we discuss the contribution of the new data to the classification of the CJF sample into source types, in particular CSO/GPS sources, and count the number of sources whose spectra are rising at 30 GHz.

## 2. OCRA-p on the Toruń 32-m telescope

The OCRA-p receiver was constructed by the University of Manchester. The basic design of the radiometer was taken from the prototype demonstrator radiometer for the Planck Low Frequency Instrument (LFI, Mandolesi et al. 2000) and is similar to the K-band receivers onboard the WMAP satellite (Jarosik et al. 2003).

Rather than switching between a source and a fixed temperature load, as in Planck, OCRA-p switches between two closely spaced horns observing the sky continuously. When mounted on the Toruń 32-m, the two beams are separated by 3.1', a figure set by the optics of the telescope, and therefore both receive very similar atmospheric contributions from the near-field. A phase switch in one of the radiometer arms alternates the input signals between the two output channels and, by taking the difference between the channels and between switch states, it is possible to reduce the effects of both the atmospheric and gain fluctuations in the back-end amplifiers. The differencing scheme produces positive and negative beams (see Figure 1) and this is characterised by an s-shaped response. The nominal specifications for OCRA-p are given in Table 1. The construction and commissioning of the instrument is described in detail in Lowe (2005).

The switching scheme works well despite the low altitude (200 m) of the Toruń site. OCRA-p has been able to make good observations even during summer nights.

## 3. Observations

At the time these observations were taken (**April - August 2005**), the pointing accuracy of the 32-m radio telescope was dependent on elevation and azimuth in a complex manner. The pointing accuracy was best at relatively high elevations ( $50^\circ - 70^\circ$ ) and so it was desirable to confine most of our observations to this range. A pointing observation was incorporated within the overall observing strategy for each source. For each source measurement, an elevation scan of the source was first recorded.

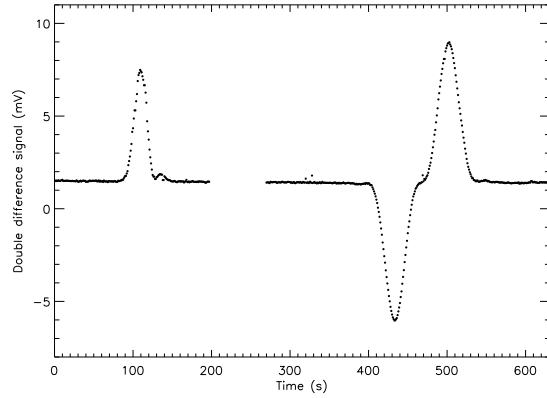


**Fig. 1.** A figure to illustrate the scan strategy. An initial pointing correction is found by fitting a Gaussian function to an elevation scan (left) through the source. This correction is applied to the telescope position and then an azimuthal scan is performed. The initial pointing error can be seen in the difference in amplitudes of the beams in the two scans. The elevation scan did not pass through the centre of the source, so the amplitude is lower than the azimuth scan (right) with the elevation correction.

Custom software then fitted a Gaussian function to these data, in real time, and the central point was used to generate a pointing correction for the elevation coordinate. With the calculated elevation correction an azimuthal scan was then performed. The length of the scan was chosen to be several beam spacings in extent to allow for azimuthal pointing errors and to determine a good baseline. Figure 1 shows an indicative illustration of the scan strategy. To the left is the preliminary elevation scan and to the right, the azimuthal scan. The s-shaped response, generated as the source passes through each beam in turn, can clearly be seen in the azimuthal scan.

For each azimuthal scan a baseline and two independent Gaussian functions were fitted for each beam. At this stage, every observation that was significantly affected by atmospheric fluctuations, or that showed large asymmetries in the amplitudes of the beams, was rejected.

The amplitudes of the fitted Gaussian functions are directly related to the strength of the source. To convert the measured signal to a flux density it is necessary to calibrate against a source of known strength. Our primary flux calibrator was chosen to be the planetary nebula NGC 7027 which has an optical diameter of  $\sim 15''$  and is circumpolar at the latitude of Toruń. There is a recent absolute temperature calibration of NGC 7027 performed by Mason et al. (1999) who report a flux density of  $5.45 \pm 0.20$  Jy at 32 GHz. Assuming a spectral index of  $-0.1 \pm 0.1$  and estimating the beam dilution factor, using a simple geometric model of the emission created from 6-cm radio maps from Bryce et al. (1997), gives an expected flux density of  $5.46 \pm 0.20$  Jy at 30 GHz. All the final flux density values have been scaled to this figure.

Although NGC 7027 is circumpolar, it is not always at a suitable elevation and can be too far from the CJF target sources for reliable calibration. A network of secondary flux density calibrators was therefore generated. The secondary calibrators were: 0010+405, 0016+731, 0109+351, 0309+411, 0633+734, 0642+449, 0821+394, 0833+585, 0955+476, 1044+719, 1144+402, 1418+546, 1638+398, 1758+388, 2007+777, 2021+614. Several of these sources show long-term variability in their emission, however the level of intrinsic

intra-day variations did not contribute significantly to our final error budget.

Every three to six target observations, a secondary calibrator source was observed. The secondary calibrator measurements were calibrated using the measurements of NGC 7027. **The final flux densities take into account atmospheric absorption (estimated uncertainty  $\sim 2\%$  in the correction) and a gain-elevation correction ( $\sim 2.5\%$ ).** Uncertainties in these corrections as well as pointing errors ( $< 1\%$  for this observing method), uncertainties in the extrapolated flux density of NGC 7027 (3.6%) and in the secondary calibration ( $\sim 6\%$ ) have been incorporated into the final error budget. The typical uncertainty for a single flux density measurement is in the range 8–10%. Since six or more measurements were usually made for each source and the errors are independent, the final uncertainties are typically around 5%.

The flux density measurements are made over a 6 GHz bandwidth (27–33 GHz). We note that sources with spectral curvature that is different to the primary calibrator will have systematic errors in their flux densities. However, as NGC 7027 and the majority of our sample are flat-spectrum, we neglect this effect given the other uncertainties.

## 4. Results

The final 30-GHz flux densities are given in Table 2. Column (1) gives the IAU B1950 source name for consistency with previous CJF observations by other authors. The J2000 coordinates are given in Columns (2) and (3) and are taken from Taylor et al. (1996). The flux densities at 5 GHz, Column (4), are also taken from Taylor et al. (1996) and are reproduced for comparison with those measured by OCRA-p at 30 GHz in Column (5). Column (6) lists the associated uncertainties in the 30 GHz flux densities. The spectral index between 1.4 GHz and 5 GHz,  $\alpha_{1.4}^5$ , from Taylor et al. (1996) is given in Column (7) and the spectral index between 5 GHz and 30 GHz,  $\alpha_5^{30}$ , is given in Column (8). **The formal uncertainty on  $\alpha_5^{30}$ , given the typical uncertainties in both the 5 and 30 GHz measurements, is  $< 0.1$ . We note however, that the uncertainties for a few objects may be larger due to variability and the fact that the observations at 5 and 30 GHz are not co-eval.** The morphology, from inspection of VLBI maps, is given in Column (9).

To classify the spectral behaviour of the CJF sources, the latest spectral information was obtained from NED. For the spectral plots including the 30 GHz values, refer to <http://www.manchester.ac.uk/jodrellbank/research/ocra/cjf/>

## 5. Discussion

Figure 2 shows the distribution of spectral indices as given in Table 2. The distribution can be compared with Figure 1b in Taylor et al. (1996) which shows the spectral index distribution between 1.4 GHz and 4.85 GHz,  $\alpha_{1.4}^{4.85}$ . The major difference is the shift to lower spectral indices mainly due to the spectral index cut-off of the CJF sample ( $-0.5$  at 5 GHz). A significant fraction ( $\sim 31\%$ ) of sources are seen to have spectral indices,  $\alpha_5^{30}$  steeper than  $-0.5$ . This is the expected behaviour of GPS sources peaking at or above  $\sim 5$  GHz. Looking at the spectra as a whole we classify 42 ( $\sim 14\%$ ) sources as having GPS spectra (0018+729; 0102+480; 0108+388; 0145+386; 0248+430; 0615+820; 0627+532; 0636+680; 0646+600; 0700+470; 0710+439; 0711+356; 0740+768; 0859+681; 0900+520; 0950+748; 1031+567; 1107+607; 1144+352; 1205+544;

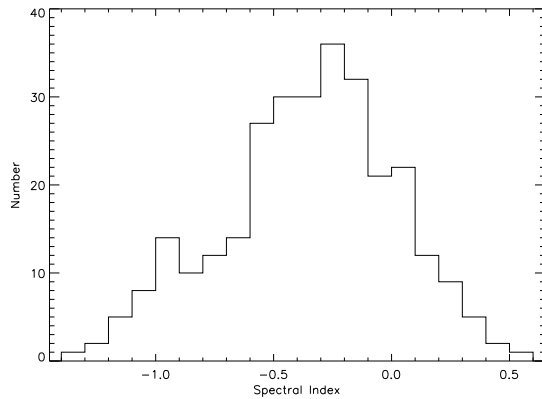


Fig. 2. Distribution of spectral indices calculated between 5 GHz and 30 GHz. Using data from Table 2.

1206+415; 1223+395; 1226+373; 1312+533; 1333+459; 1337+637; 1342+663; 1355+441; 1356+478; 1413+373; 1442+637; 1526+670; 1534+501; 1543+480; 1550+582; 1622+665; 1755+578; 1758+388; 1826+796; 1946+708; 2352+495; 2356+385). We note that O'Dea (1998) found that  $\sim 10\%$  of sources, selected at 5 GHz, were GPS. Our results on a 5 GHz sample, selected against sources with steep spectra, are therefore in rough accord with O'Dea (1998) statistics.

There are a total of 49 sources ( $\sim 17\%$ ) which have  $\alpha_5^{30} > 0$  and can therefore be considered to have rising spectra. Only one source, 0109+351, has  $\alpha_5^{30} > 0.5$  compared to the 41 which have  $\alpha_{1.4}^5 > 0.5$  (Taylor et al. 1996). We do not, however, claim that this is clear evidence for a decrease in the number of steeply rising sources with increasing frequency but is, we suspect, simply a result of selection bias. **If for example we had selected sources at 30 GHz we assert that we would have found many more sources with spectra steeply rising between 5 and 30 GHz.** The same effect is seen in the results reported by Bolton et al. (2004) on the  $\alpha_{15}^{43}$  spectral index distribution, for sources selected at 15 GHz from the 9C survey; these indicate that around 1% of these sources have spectra rising faster than 0.5 between 15 GHz and 43 GHz.

The number of sources with steeply rising spectra in high frequency surveys is of great interest because sources act as a confusing foreground to CMB studies and to SZ decrement measurements. Waldram et al. (2003) have made surveys of areas of sky at 15 GHz coincident with small area CMB fields studied with the Very Small Array (VSA, Scott et al. 2003). OCRA-p measurements of these sources will be reported elsewhere. However, with the higher sensitivity over the whole sky which will be achieved by Planck, wide-field 30 GHz surveys are urgently required. We plan to install a 30 GHz 16-beam array (OCRA-F) on the Toruń telescope in 2008 and one of its main tasks will be to do such a blind survey.

Further work on spectral energy distributions is in progress and is planned for the future. Observations of 145 (130 have signal-to-noise greater than 3) of the CJF sources have been made at  $850 \mu\text{m}$  with SCUBA and will be reported in Anton et al. (2007). With an improved telescope control system it will be possible to improve greatly the speed and accuracy of flux density measurements made with OCRA-p. This will facilitate a much larger programme of blazar flux density measurements and variability monitoring to be undertaken in support of the GLAST satellite which will be launched later this year.

*Acknowledgements.* We gratefully acknowledge the financial support of the Royal Society Paul Instrument Fund which allowed us to construct the 30 GHz receiver. We are also grateful to the Polish Ministry of Science and Higher Education (grant KBN 5 P03D 024 21) which provided support for operating the receiver on the Toruń 32-m telescope. This research has made use of the NASA/IPAC Extragalactic Database (NED) which is operated by the Jet Propulsion Laboratory, California Institute of Technology, under contract with the National Aeronautics and Space Administration. S.R. Lowe was supported by a PPARC studentship.

## References

- Antón, S. & Browne, I. W. A. 2005, MNRAS, 356, 225  
 Bolton, R. C., Cotter, G., Pooley, G. G., et al. 2004, MNRAS, 354, 485  
 Britzen, S., Brinkmann, W., Vermeulen, R. C., et al. 2002, in Proceedings of the 6th EVN Symposium, ed. E. Ros, R. W. Porcas, A. P. Lobanov, & J. A. Zensus, 99  
 Bryce, M., Pedlar, A., Muxlow, T., Thomasson, P., & Mellem, G. 1997, MNRAS, 284, 815  
 Fossati, G., Maraschi, L., Celotti, A., Comastri, A., & Ghisellini, G. 1998, MNRAS, 299, 433  
 Ghisellini, G., Celotti, A., & Costamante, L. 2002, A&A, 386, 833  
 Jarosik, N., Bennett, C. L., Halpern, M., et al. 2003, ApJS, 145, 413  
 Kuehr, H., Pauliny-Toth, I. I. K., Witzel, A., & Schmidt, J. 1981, AJ, 86, 854  
 Lancaster, K., Birkinshaw, M., Gawroński, M. P., et al. 2007, MNRAS, 378, 673  
 Lowe, S. R. 2005, PhD thesis, University of Manchester  
 Mandolesi, N., Bersanelli, M., Burigana, C., & Villa, F. 2000, Astrophysical Letters Communications, 37, 151  
 Mason, B. S., Leitch, E. M., Myers, S. T., Cartwright, J. K., & Readhead, A. C. S. 1999, AJ, 118, 2908  
 O'Dea, C. P. 1998, PASP, 110, 493  
 Pearson, T. & Readhead, A. 1988, ApJ, 328, 114  
 Polatidis, A., Wilkinson, P., Xu, W., et al. 1995, ApJS, 98, 1  
 Readhead, A. C. S., Taylor, G. B., Pearson, T. J., & Wilkinson, P. N. 1996a, ApJ, 460, 634  
 Readhead, A. C. S., Taylor, G. B., Xu, W., et al. 1996b, ApJ, 460, 612  
 Rossetti, A., Mantovani, F., Dallacasa, D., Fanti, C., & Fanti, R. 2005, A&A, 434, 449  
 Scott, P. F., Carreira, P., Cleary, K., et al. 2003, MNRAS, 341, 1076  
 Taylor, G. B., Vermeulen, R. C., Pearson, T. J., et al. 1994, ApJS, 95, 345  
 Taylor, G. B., Vermeulen, R. C., Readhead, A. C. S., et al. 1996, ApJS, 107, 37  
 Waldram, E. M., Pooley, G. G., Grainge, K. J. B., et al. 2003, MNRAS, 342, 915  
 Wilkinson, P., Polatidis, A., Readhead, A., Xu, W., & Pearson, T. 1994, ApJ, 432, L87

**Table 2.** 30-GHz flux density measurements with OCRA-p and the Toru'n 32-m telescope.; col. (1) gives the IAU B1950 source name; cols. (2) and (3) give the J2000 positions; col. (4) gives the flux densities at 5 GHz; col. (5) gives the 30-GHz OCRA-p flux densities; col. (6) gives the associated uncertainty; cols. (7) and (8) give the calculated spectral indices between 1.4 and 5 GHz ( $\alpha_{1.4}^5$  taken from Taylor et al. 1996), and between 5 and 30 GHz ( $\alpha_5^{30}$ ); col. (9) indicates the VLBI morphology where c=compact, cj=core-jet, d=double, cso=compact symmetric object, mso=medium symmetric object, t=triple, g=gravitational lens.

Name (1)	R.A. (J2000) (2)	Declination (J2000) (3)	$S_{5.0}$ (Jy) (4)	$S_{30}$ (Jy) (5)	$\Delta S_{30}$ (Jy) (6)	$\alpha_{1.4}^5$ (7)	$\alpha_5^{30}$ (8)	Morph. (9)
0003+380	00 05 57.2	38 20 15	0.549	0.654	0.037	-0.07	0.10	cj
0010+405	00 13 31.1	40 51 37	1.040	0.775	0.032	-0.43	-0.16	cj
0014+813	00 17 08.5	81 35 08	0.551 <sup>a</sup>	0.629	0.030	-0.17 <sup>a</sup>	0.07	cj
0016+731	00 19 45.8	73 27 30	1.712	1.612	0.067	0.54	-0.03	cj
0018+729	00 21 27.4	73 12 41	0.397	0.071	0.004	-0.42	-0.96	cj
0022+390	00 25 26.2	39 19 35	0.663	0.282	0.020	-0.11	-0.48	cj
0035+367	00 37 46.1	36 59 10	0.482	0.184	0.010	-0.47	-0.54	cj
0035+413	00 38 24.8	41 37 06	1.114	0.395	0.020	0.73	-0.58	cj
0102+480	01 05 49.9	48 19 03	1.088	0.428	0.024	0.15	-0.52	cj/c
0108+388	01 11 37.3	39 06 28	1.321	0.200	0.010	0.92	-1.05	cso
0109+351	01 12 12.9	35 22 19	0.362	1.014	0.043	0.00	0.57	cj
0110+495	01 13 27.0	49 48 24	0.710	0.570	0.032	0.30	-0.12	cj
0133+476	01 36 58.6	47 51 29	1.816	3.271	0.171	0.21	0.33	cj
0145+386	01 48 24.4	38 54 05	0.370	0.229	0.017	0.18	-0.27	cj?
0151+474	01 54 56.3	47 43 26	0.505	0.500	0.026	0.28	-0.01	cj
0153+744	01 57 35.0	74 42 43	1.549	0.148	0.007	-0.23	-1.31	cj
0205+722	02 09 51.8	72 29 26	0.560	0.715	0.037	-0.32	0.14	cj
0212+735	02 17 30.8	73 49 32	2.278	2.726	0.136	-0.11	0.10	cj
0218+357	02 21 05.5	35 56 13	1.498	0.846	0.043	0.02	-0.32	g
0219+428	02 22 39.6	43 02 07	0.806	0.801	0.043	0.00	-0.00	cj
0227+403	02 30 45.7	40 32 53	0.436	0.421	0.022	-0.00	-0.02	cj
0248+430	02 51 34.5	43 15 15	1.414	0.503	0.025	0.41	-0.58	cj/t
0249+383	02 53 08.9	38 35 24	0.450	0.286	0.015	-0.43	-0.25	cj
0251+393	02 54 42.6	39 31 34	0.408	0.321	0.019	0.25	-0.13	cj
0256+424	02 59 37.7	42 35 49	0.366	0.132	0.009	-0.41	-0.57	cj
0307+380	03 10 49.9	38 14 53	0.760	0.686	0.034	1.52	-0.06	c
0309+411	03 13 02.0	41 20 01	0.516	1.019	0.042	0.08	0.38	cj
0316+413	03 19 48.2	41 30 42	42.370	10.803	0.507	0.54	-0.76	cj
0340+362	03 43 29.0	36 22 12	0.376	0.232	0.012	0.23	-0.27	cj?
0344+405	03 47 60.0	40 43 58	0.478	0.099	0.006	-0.47	-0.88	d
0346+800	03 54 46.1	80 09 28	0.396 <sup>a</sup>	0.272	0.015	-0.25 <sup>a</sup>	-0.21	cj
0402+379	04 05 49.3	38 03 32	0.937	0.285	0.016	-0.38	-0.66	cj
0424+670	04 29 06.0	67 10 16	0.362	0.080	0.004	-0.47	-0.84	c?
0444+634	04 49 23.3	63 32 09	0.606	0.699	0.034	0.39	0.08	cj
0454+844	05 08 42.4	84 32 04	1.398 <sup>a</sup>	0.266	0.015	0.40 <sup>a</sup>	-0.93	cj
0537+531	05 41 16.2	53 12 24	0.665	0.230	0.011	0.01	-0.59	cj
0546+726	05 52 53.0	72 40 45	0.401	0.074	0.005	-0.16	-0.94	cj?
0554+580	05 59 13.4	58 04 03	0.906	0.496	0.024	0.70	-0.34	cj
0600+442	06 04 35.6	44 13 58	0.705	0.212	0.014	-0.42	-0.67	cj
0602+673	06 07 52.7	67 20 55	0.657	0.897	0.049	0.62	0.17	cj
0604+728	06 10 48.9	72 48 53	0.654	0.273	0.015	-0.35	-0.49	cj
0609+607	06 14 23.9	60 46 21	1.059	0.375	0.021	-0.00	-0.58	cj
0615+820	06 26 03.0	82 02 25	0.999 <sup>a</sup>	0.343	0.021	-0.03 <sup>a</sup>	-0.60	c
0620+389	06 24 19.0	38 56 48	0.811	0.450	0.028	-0.32	-0.33	cj
0621+446	06 25 18.3	44 40 01	0.369	0.211	0.013	0.63	-0.31	c
0627+532	06 31 34.7	53 11 27	0.485	0.104	0.006	-0.40	-0.86	cj
0633+596	06 38 02.9	59 33 22	0.482	0.691	0.037	0.58	0.20	cj
0633+734	06 39 22.0	73 24 58	0.748	0.787	0.032	-0.30	0.03	cj
0636+680	06 42 04.3	67 58 35	0.499	0.113	0.006	1.06	-0.83	c
0641+393	06 44 53.7	39 14 47	0.453	0.322	0.016	0.17	-0.19	cj
0642+449	06 46 32.0	44 51 16	1.191	2.420	0.100	0.55	0.40	cj?
0646+600	06 50 31.3	60 01 44	0.920	0.470	0.024	0.58	-0.37	d
0650+371	06 53 58.3	37 05 40	0.977	0.619	0.036	0.40	-0.25	cj
0650+453	06 54 23.7	45 14 23	0.420	0.516	0.027	-0.27	0.11	cj
0651+410	06 55 10.0	41 00 10	0.425	0.284	0.015	0.27	-0.22	cj?
0700+470	07 04 09.6	47 00 56	0.443	0.120	0.007	-0.49	-0.73	cj

**Table 2.** continued.

Name (1)	R.A. (J2000) (2)	Declination (J2000) (3)	$S_{5.0}$ (Jy) (4)	$S_{30}$ (Jy) (5)	$\Delta S_{30}$ (Jy) (6)	$\alpha_{1.4}^5$ (7)	$\alpha_5^{30}$ (8)	Morph. (9)
0702+612	07 07 00.6	61 10 11	0.370	0.433	0.024	0.10	0.09	cj
0707+476	07 10 46.1	47 32 11	0.906	0.739	0.038	-0.06	-0.11	cj
0710+439	07 13 38.2	43 49 17	1.629	0.423	0.024	-0.09	-0.75	cso
0711+356	07 14 24.8	35 34 39	0.901	0.171	0.011	-0.36	-0.93	d
0714+457	07 17 51.9	45 38 03	0.480	0.995	0.052	0.13	0.41	cj
0716+714	07 21 53.4	71 20 36	0.788	0.546	0.029	-0.02	-0.20	cj
0718+793	07 26 11.7	79 11 31	0.631 <sup>a</sup>	0.382	0.022	0.03 <sup>a</sup>	-0.28	cj
0724+571	07 28 49.6	57 01 24	0.393	0.389	0.021	-0.03	-0.01	cj
0727+409	07 30 51.3	40 49 50	0.468	0.093	0.005	0.10	-0.90	cj
0730+504	07 33 52.5	50 22 09	0.890	0.428	0.026	0.66	-0.41	cj
0731+479	07 35 02.3	47 50 08	0.533	0.256	0.015	0.17	-0.41	cj
0733+597	07 37 30.1	59 41 03	0.357	0.165	0.009	-0.34	-0.43	cj
0738+491	07 42 02.8	49 00 15	0.352	0.319	0.019	1.05	-0.05	cj?
0740+768	07 47 14.6	76 39 17	0.592 <sup>a</sup>	0.336	0.020	0.87 <sup>a</sup>	-0.32	d?
0743+744	07 49 22.5	74 20 41	0.479	0.306	0.016	0.24	-0.25	cj
0746+483	07 50 20.4	48 14 53	0.860	0.422	0.030	0.21	-0.40	cj
0749+426	07 53 03.3	42 31 30	0.461	0.058	0.004	-0.33	-1.16	cj/d?
0749+540	07 53 01.4	53 52 59	0.877	0.913	0.051	0.08	0.02	cj
0800+618	08 05 18.2	61 44 23	0.981	0.539	0.029	0.25	-0.33	cj
0803+452	08 06 33.5	45 04 32	0.414	0.350	0.018	0.05	-0.09	cj
0804+499	08 08 39.7	49 50 36	1.222	1.599	0.113	0.25	0.15	cj
0805+410	08 08 56.7	40 52 44	0.743	0.694	0.036	0.57	-0.04	cj
0806+573	08 11 00.6	57 14 12	0.405	0.418	0.023	-0.04	0.02	cj
0812+367	08 15 25.9	36 35 15	0.980	0.414	0.022	-0.03	-0.48	cj
0814+425	08 18 16.0	42 22 45	1.891	0.595	0.036	0.20	-0.65	cj
0820+560	08 24 47.2	55 52 42	1.199	0.595	0.031	-0.05	-0.39	cj
0821+394	08 24 55.5	39 16 41	1.012	1.179	0.055	-0.24	0.09	cj
0821+621	08 25 38.6	61 57 28	0.615	0.294	0.017	-0.05	-0.41	d
0824+355	08 27 38.6	35 25 05	0.746	0.294	0.016	-0.12	-0.52	cj
0831+557	08 34 54.9	55 34 21	5.780	0.633	0.034	-0.23	-1.23	cj
0833+416	08 36 36.9	41 25 54	0.385	0.306	0.016	-0.08	-0.13	cj
0833+585	08 37 22.4	58 25 01	0.669	0.832	0.036	0.09	0.12	cj
0836+710	08 41 24.4	70 53 42	2.423	1.309	0.064	-0.44	-0.34	cj
0843+575	08 47 28.1	57 23 38	0.384	0.043	0.004	0.24	-1.22	cj
0847+379	08 50 24.7	37 47 09	0.382	0.287	0.016	-0.37	-0.16	cj
0850+581	08 54 42.0	57 57 29	1.187	0.299	0.017	-0.14	-0.77	cj
0859+470	09 03 04.0	46 51 04	1.285	0.823	0.044	-0.45	-0.25	cj
0859+681	09 03 53.2	67 57 22	0.751	0.272	0.016	0.19	-0.57	cj
0900+520	09 03 58.6	51 51 00	0.395	0.182	0.010	0.16	-0.43	cj?
0902+490	09 05 27.5	48 50 49	0.547	0.096	0.005	-0.12	-0.97	cj?
0917+449	09 20 58.5	44 41 53	1.033	1.704	0.101	0.22	0.28	cj
0917+624	09 21 36.2	62 15 52	1.322	0.813	0.040	0.06	-0.27	d
0923+392	09 27 03.0	39 02 20	7.480	5.726	0.388	0.80	-0.15	cj
0925+504	09 29 15.4	50 13 35	0.558	0.469	0.027	0.58	-0.10	cj
0927+352	09 30 55.3	35 03 37	0.383	0.294	0.018	-0.08	-0.15	cj
0929+533	09 32 41.2	53 06 33	0.384	0.141	0.008	-0.26	-0.56	cj
0930+493	09 34 15.8	49 08 21	0.574	0.161	0.009	-0.19	-0.71	cj
0942+468	09 45 42.1	46 36 50	0.354	0.192	0.010	0.19	-0.34	cj
0945+408	09 48 55.3	40 39 44	1.592	1.018	0.076	0.05	-0.25	cj
0945+664	09 49 12.2	66 14 59	1.407	0.270	0.016	-0.36	-0.92	mso <sup>b</sup>
0949+354	09 52 32.0	35 12 52	0.403	0.216	0.013	0.12	-0.35	cj
0950+748	09 54 47.4	74 35 57	0.738	0.106	0.007	-0.37	-1.08	cj
0954+556	09 57 38.2	55 22 57	2.270	1.016	0.076	-0.22	-0.45	mso <sup>b</sup>
0954+658	09 58 47.2	65 33 54	1.417	1.002	0.075	0.61	-0.19	cj
0955+476	09 58 19.7	47 25 07	0.834	1.389	0.059	0.15	0.28	cj
1003+830	10 10 15.8	82 50 14	0.716 <sup>a</sup>	0.422	0.034	-0.14 <sup>a</sup>	-0.30	cj
1010+350	10 13 49.6	34 45 50	0.597	0.420	0.025	0.28	-0.20	cj
1014+615	10 17 25.9	61 16 27	0.631	0.302	0.016	0.44	-0.41	cj
1015+359	10 18 11.0	35 42 39	0.587	1.007	0.058	-0.34	0.30	cj
1020+400	10 23 11.6	39 48 15	0.785	0.571	0.029	-0.31	-0.18	cj

**Table 2.** continued.

Name (1)	R.A. (J2000) (2)	Declination (J2000) (3)	$S_{5.0}$ (Jy) (4)	$S_{30}$ (Jy) (5)	$\Delta S_{30}$ (Jy) (6)	$\alpha_{1.4}^5$ (7)	$\alpha_5^{30}$ (8)	Morph. (9)
1030+398	10 33 22.1	39 35 51	0.645	0.128	0.007	0.42	-0.90	cj
1030+415	10 33 03.7	41 16 06	0.485	0.617	0.036	-0.37	0.13	cj
1030+611	10 33 51.4	60 51 07	0.579	0.490	0.026	-0.22	-0.09	cj
1031+567	10 35 07.0	56 28 46	1.200	0.184	0.010	-0.30	-1.05	cso
1038+528	10 41 46.8	52 33 28	0.709	0.393	0.020	-0.00	-0.33	cj
1039+811	10 44 23.1	80 54 39	1.144 <sup>a</sup>	0.864	0.064	0.40 <sup>a</sup>	-0.16	cj
1041+536	10 44 10.7	53 22 20	0.481	0.370	0.019	-0.10	-0.15	cj
1044+719	10 48 27.6	71 43 35	2.410	2.480	0.109	1.06	0.02	c
1053+704	10 56 53.6	70 11 45	0.675	1.073	0.060	0.08	0.26	cj
1053+815	10 58 11.5	81 14 32	0.770 <sup>a</sup>	0.643	0.047	-0.36 <sup>a</sup>	-0.10	cj
1058+629	11 01 53.4	62 41 50	0.700	0.105	0.006	0.12	-1.06	cj
1058+726	11 01 48.8	72 25 37	0.953	0.493	0.030	-0.33	-0.37	cj
1101+384	11 04 27.3	38 12 31	0.722	0.393	0.020	-0.11	-0.34	cj
1105+437	11 08 23.5	43 30 53	0.375	0.382	0.023	0.27	0.01	cj
1106+380	11 09 28.9	37 44 30	0.867	0.240	0.013	-0.38	-0.72	cj
1107+607	11 10 13.1	60 28 42	0.404	0.053	0.004	0.12	-1.13	cj
1124+455	11 26 57.7	45 16 06	0.355	0.060	0.004	-0.26	-0.99	cj
1124+571	11 27 40.1	56 50 14	0.597	0.237	0.014	-0.20	-0.52	cj
1125+596	11 28 13.3	59 25 14	0.393	0.605	0.034	0.06	0.24	c
1128+385	11 30 53.3	38 15 18	0.746	1.094	0.055	-0.18	0.21	cj
1143+590	11 46 26.9	58 48 34	0.674	0.422	0.025	0.70	-0.26	cj
1144+352	11 47 22.1	35 01 07	0.663	0.182	0.010	-0.04	-0.72	cj
1144+402	11 46 58.3	39 58 34	0.739	1.129	0.047	-0.17	0.24	cj
1144+542	11 46 44.2	53 56 43	0.484	0.391	0.024	0.14	-0.12	cj
1146+596	11 48 50.4	59 24 56	0.627	0.362	0.022	0.32	-0.31	cj/cso
1150+812	11 53 12.5	80 58 29	1.181 <sup>a</sup>	1.522	0.091	-0.09 <sup>a</sup>	0.14	cj
1151+408	11 53 54.7	40 36 52	0.380	0.246	0.013	-0.48	-0.24	cj?
1155+486	11 58 26.8	48 25 16	0.445	0.214	0.013	-0.07	-0.41	cj
1205+544	12 08 27.5	54 13 19	0.397	0.091	0.006	-0.12	-0.82	d?
1206+415	12 09 22.8	41 19 41	0.515	0.197	0.010	0.37	-0.54	c
1213+350	12 15 55.6	34 48 15	1.152	0.540	0.030	-0.32	-0.42	cj
1216+487	12 19 06.4	48 29 56	0.680	0.670	0.040	-0.18	-0.01	cj
1218+444	12 21 27.0	44 11 29	0.478	0.206	0.013	-0.18	-0.47	cj
1221+809	12 23 40.5	80 40 04	0.518 <sup>a</sup>	0.392	0.028	0.43 <sup>a</sup>	-0.16	cj
1223+395	12 25 50.6	39 14 22	0.438	0.154	0.009	-0.16	-0.58	cj
1226+373	12 28 47.4	37 06 12	0.953	0.168	0.009	1.26	-0.97	cj
1239+376	12 42 09.8	37 20 05	0.446	0.203	0.012	-0.16	-0.44	cj
1240+381	12 42 51.4	37 51 00	0.768	0.375	0.022	0.59	-0.40	cj
1246+586	12 48 18.8	58 20 28	0.414	0.123	0.008	0.43	-0.68	cj
1250+532	12 53 11.9	53 01 11	0.396	0.380	0.023	-0.24	-0.02	cj
1254+571	12 56 14.2	56 52 25	0.419	0.129	0.009	0.29	-0.66	cj?
1258+507	13 00 41.2	50 29 36	0.391	0.280	0.015	-0.23	-0.19	cj
1300+580	13 02 52.5	57 48 37	0.758	0.759	0.047	0.72	0.00	cj
1305+804	13 06 05.7	80 08 20	0.375 <sup>a</sup>	0.108	0.012	-0.47 <sup>a</sup>	-0.69	cj
1306+360	13 08 23.7	35 46 37	0.437	0.510	0.029	0.54	0.09	cj
1307+562	13 09 09.8	55 57 38	0.416	0.279	0.018	0.27	-0.22	cj
1308+471	13 10 53.6	46 53 52	0.393	0.281	0.017	1.08	-0.19	cj?
1309+555	13 11 03.2	55 13 54	0.677	0.278	0.017	0.91	-0.50	cj
1312+533	13 14 43.8	53 06 27	0.433	0.066	0.004	0.49	-1.05	cj
1321+410	13 24 12.1	40 48 11	0.413	0.057	0.004	0.11	-1.11	d
1322+835	13 21 45.6	83 16 13	0.506 <sup>a</sup>	0.194	0.015	0.23 <sup>a</sup>	-0.54	cj
1323+800	13 23 51.6	79 42 51	0.458 <sup>a</sup>	0.307	0.019	0.22 <sup>a</sup>	-0.22	cj
1325+436	13 27 21.0	43 26 27	0.533	0.194	0.011	-0.22	-0.56	cj
1333+459	13 35 22.0	45 42 38	0.598	0.230	0.013	0.51	-0.53	cj?
1333+589	13 35 25.9	58 44 00	0.820	0.200	0.011	-0.07	-0.79	d
1335+552	13 37 49.6	55 01 02	0.811	0.378	0.023	0.10	-0.43	cj
1337+637	13 39 23.8	63 28 58	0.431	0.080	0.005	-0.12	-0.94	cj
1342+663	13 44 08.7	66 06 11	0.510	0.300	0.017	-0.43	-0.30	cj
1347+539	13 49 34.7	53 41 17	0.635	0.438	0.024	-0.46	-0.21	cj
1355+441	13 57 40.7	43 53 59	0.464	0.101	0.007	-0.33	-0.85	cj

**Table 2.** continued.

Name (1)	R.A. (J2000) (2)	Declination (J2000) (3)	$S_{5.0}$ (Jy) (4)	$S_{30}$ (Jy) (5)	$\Delta S_{30}$ (Jy) (6)	$\alpha_{1.4}^5$ (7)	$\alpha_5^{30}$ (8)	Morph. (9)
1356+478	13 58 40.7	47 37 58	0.428	0.070	0.006	-0.26	-1.01	d/cso?
1357+769	13 57 55.4	76 43 21	0.844 <sup>a</sup>	0.698	0.043	0.62 <sup>a</sup>	-0.11	cj
1413+373	14 15 28.5	37 06 21	0.383	0.060	0.004	0.04	-1.03	cj
1415+463	14 17 08.2	46 07 05	0.904	0.489	0.026	-0.09	-0.34	cj
1417+385	14 19 46.6	38 21 48	0.871	0.543	0.032	0.16	-0.26	cj
1418+546	14 19 46.6	54 23 14	1.707	0.781	0.033	0.07	-0.44	cj
1421+482	14 23 06.2	48 02 10	0.536	0.249	0.014	0.31	-0.43	cj
1424+366	14 26 37.1	36 25 09	0.429	0.278	0.015	0.62	-0.24	cj
1427+543	14 29 21.9	54 06 11	0.718	0.178	0.009	-0.18	-0.78	cj
1432+422	14 34 05.7	42 03 16	0.353	0.109	0.007	0.19	-0.66	cj
1435+638	14 36 45.8	63 36 37	0.795	0.541	0.032	-0.44	-0.21	cj
1438+385	14 40 22.3	38 20 13	0.944	0.321	0.018	-0.06	-0.60	cj
1442+637	14 43 58.6	63 32 26	0.456	0.088	0.006	-0.32	-0.92	cj
1448+762	14 48 28.8	76 01 11	0.683 <sup>a</sup>	0.501	0.028	0.33 <sup>a</sup>	-0.17	cj
1456+375	14 58 44.8	37 20 21	0.591	0.151	0.008	0.45	-0.76	cj
1459+480	15 00 48.7	47 51 15	0.489	0.282	0.016	0.16	-0.31	cj
1504+377	15 06 09.5	37 30 51	1.003	0.555	0.034	-0.13	-0.33	cj
1505+428	15 06 53.0	42 39 23	0.404	0.547	0.030	-0.06	0.17	cj
1526+670	15 26 42.9	66 50 54	0.417	0.078	0.005	-0.02	-0.94	cj
1531+722	15 31 33.6	72 06 41	0.452	0.161	0.009	-0.30	-0.58	cj
1534+501	15 35 52.0	49 57 39	0.359	0.169	0.010	0.35	-0.42	c
1543+480	15 45 08.5	47 51 54	0.441	0.078	0.006	-0.32	-0.97	d/cso
1543+517	15 45 02.8	51 35 00	0.544	0.093	0.005	0.09	-0.99	cj
1545+497	15 47 21.1	49 37 05	0.549	0.163	0.010	-0.42	-0.68	c
1547+507	15 49 17.5	50 38 05	0.724	0.738	0.039	0.06	0.01	cj
1550+582	15 51 58.2	58 06 44	0.367	0.254	0.014	0.38	-0.21	cj
1619+491	16 20 31.2	49 01 53	0.469	0.214	0.012	0.00	-0.44	cj
1622+665	16 23 04.5	66 24 01	0.520	0.122	0.007	0.74	-0.81	cj?
1623+578	16 24 24.8	57 41 16	0.590	0.424	0.025	0.13	-0.18	cj
1624+416	16 25 57.7	41 34 40	1.362	0.521	0.030	-0.17	-0.54	cj
1629+495	16 31 16.5	49 27 39	0.394	0.458	0.026	0.16	0.08	cj
1633+382	16 35 15.5	38 08 04	3.189	2.976	0.173	0.41	-0.04	cj
1636+473	16 37 45.1	47 17 33	1.330	1.031	0.053	0.27	-0.14	cj
1637+574	16 38 13.5	57 20 23	1.807	1.317	0.071	0.30	-0.18	c
1638+398	16 40 29.6	39 46 46	1.285	0.612	0.025	0.53	-0.41	cj?
1638+540	16 39 39.8	53 57 47	0.369	0.172	0.011	0.14	-0.43	cj
1641+399	16 42 58.8	39 48 36	8.363	4.929	0.287	0.05	-0.30	cj
1642+690	16 42 07.8	68 56 39	1.516	2.746	0.128	0.00	0.33	d/cj?
1645+410	16 46 56.9	40 59 17	0.388	0.185	0.009	0.16	-0.41	cj
1645+635	16 45 58.6	63 30 10	0.444	0.410	0.023	0.31	-0.04	cj
1652+398	16 53 52.2	39 45 36	1.371	1.219	0.071	-0.04	-0.07	cj
1656+477	16 58 02.8	47 37 49	1.420	0.582	0.031	0.47	-0.50	cj
1656+482	16 57 46.9	48 08 33	0.847	0.697	0.045	-0.12	-0.11	cj
1656+571	16 57 20.7	57 05 53	0.844	0.487	0.027	0.04	-0.31	cj
1700+685	17 00 09.3	68 30 06	0.435	0.338	0.017	0.29	-0.14	cj
1716+686	17 16 13.9	68 36 38	0.988	0.536	0.025	0.69	-0.34	cj
1719+357	17 21 09.5	35 42 16	0.874	0.210	0.011	0.03	-0.80	cj
1722+401	17 24 05.4	40 04 36	0.532	0.619	0.037	-0.03	0.08	cj
1726+455	17 27 27.7	45 30 39	1.066	0.715	0.043	0.72	-0.22	cj
1732+389	17 34 20.6	38 57 51	0.561	1.105	0.075	-0.26	0.38	cj
1734+508	17 35 49.0	50 49 11	0.798	0.420	0.028	0.06	-0.36	d
1738+476	17 39 57.1	47 37 58	0.789	0.621	0.038	-0.04	-0.13	cj
1738+499	17 39 27.4	49 55 03	0.478	0.427	0.026	-0.13	-0.06	cj
1739+522	17 40 37.0	52 11 43	1.133	0.826	0.045	-0.44	-0.18	cj
1744+557	17 44 56.6	55 42 17	0.599	0.301	0.017	-0.17	-0.38	cj
1745+624	17 46 14.0	62 26 54	0.580	0.205	0.011	-0.22	-0.58	cj
1746+470	17 47 26.6	46 58 50	0.634	0.194	0.010	0.31	-0.66	cj?
1747+433	17 49 00.4	43 21 51	0.367	0.423	0.026	0.06	0.08	cj
1749+701	17 48 32.8	70 05 50	0.728	0.430	0.023	-0.46	-0.29	cj
1751+441	17 53 22.6	44 09 45	0.998	0.551	0.029	0.19	-0.33	cj

**Table 2.** continued.

Name (1)	R.A. (J2000) (2)	Declination (J2000) (3)	$S_{5.0}$ (Jy) (4)	$S_{30}$ (Jy) (5)	$\Delta S_{30}$ (Jy) (6)	$\alpha_{1.4}^5$ (7)	$\alpha_5^{30}$ (8)	Morph. (9)
1755+578	17 56 03.6	57 48 47	0.455	0.062	0.004	-0.37	-1.11	cj/cso?
1758+388	18 00 24.8	38 48 30	0.722	0.876	0.037	0.27	0.11	cj
1800+440	18 01 32.3	44 04 21	1.148	0.736	0.042	0.21	-0.25	cj
1803+784	18 00 45.7	78 28 04	2.633 <sup>a</sup>	1.211	0.063	0.27 <sup>a</sup>	-0.43	cj
1807+698	18 06 50.7	69 49 28	2.189	1.493	0.080	-0.03	-0.21	cj
1809+568	18 10 03.3	56 49 22	0.576	0.269	0.013	0.01	-0.42	cj
1812+412	18 14 22.7	41 13 05	0.534	0.266	0.018	-0.15	-0.39	cj
1818+356	18 20 42.1	35 40 39	0.573	0.195	0.012	-0.43	-0.60	cj
1823+568	18 24 07.1	56 51 01	1.135	1.642	0.100	-0.21	0.21	cj
1826+796	18 23 14.1	79 38 49	0.577 <sup>a</sup>	0.169	0.008	0.41 <sup>a</sup>	-0.69	cso
1828+399	18 29 56.5	39 57 34	0.353	0.266	0.014	0.80	-0.16	cj?
1834+612	18 35 19.7	61 19 40	0.590	0.202	0.011	0.22	-0.60	cj
1839+389	18 40 57.2	39 00 45	0.476	0.171	0.010	0.26	-0.57	cj?
1842+681	18 42 33.6	68 09 25	0.936	0.986	0.055	0.34	0.03	cj
1843+356	18 45 35.1	35 41 16	0.794	0.111	0.007	-0.21	-1.10	cj
1849+670	18 49 16.1	67 05 41	0.992	0.575	0.029	0.08	-0.30	cj
1850+402	18 52 30.4	40 19 06	0.535	0.382	0.025	-0.02	-0.19	cj
1851+488	18 52 28.5	48 55 47	0.351	0.196	0.011	0.15	-0.33	c
1856+737	18 54 57.3	73 51 19	0.546	0.530	0.027	-0.02	-0.02	cj
1908+484	19 09 46.6	48 34 31	0.423	0.151	0.008	-0.24	-0.57	c
1910+375	19 12 25.1	37 40 36	0.402	0.282	0.016	-0.18	-0.20	cj
1924+507	19 26 06.3	50 52 57	0.354	0.213	0.011	-0.48	-0.28	cj
1926+611	19 27 30.4	61 17 32	0.618	0.837	0.044	-0.06	0.17	cj
1928+738	19 27 48.5	73 58 01	3.561	2.961	0.159	-0.07	-0.10	cj
1936+714	19 36 03.6	71 31 31	0.391	0.235	0.012	-0.36	-0.28	cj?
1943+546	19 44 31.5	54 48 07	0.938	0.225	0.011	-0.44	-0.80	d
1946+708	19 45 53.5	70 55 48	0.645	0.217	0.011	-0.28	-0.61	cso
1950+573	19 51 07.0	57 27 17	0.476	0.226	0.011	-0.14	-0.42	cj
1954+513	19 55 42.7	51 31 48	1.610	0.891	0.047	-0.01	-0.33	cj
2005+642	20 06 17.7	64 24 45	0.739	0.234	0.012	1.14	-0.64	cj
2007+659	20 07 28.8	66 07 22	0.756	0.463	0.024	-0.24	-0.27	cj
2007+777	20 05 31.0	77 52 43	1.279 <sup>a</sup>	1.117	0.046	0.73 <sup>a</sup>	-0.08	cj
2010+723	20 09 52.3	72 29 19	0.910	0.916	0.045	-0.18	0.00	cj
2017+745	20 17 13.1	74 40 48	0.500	0.309	0.016	0.05	-0.27	cj
2021+614	20 22 06.7	61 36 58	2.743	1.433	0.060	0.20	-0.36	d?
2023+760	20 22 35.6	76 11 26	0.426 <sup>a</sup>	0.479	0.025	-0.13 <sup>a</sup>	0.07	cj
2054+611	20 55 38.8	61 22 00	0.414	0.262	0.014	-0.02	-0.26	cj
2116+818	21 14 01.2	82 04 48	0.376 <sup>a</sup>	0.224	0.012	-0.22 <sup>a</sup>	-0.29	cj
2136+824	21 33 34.1	82 39 06	0.509 <sup>a</sup>	0.161	0.009	-0.48 <sup>a</sup>	-0.64	cj
2138+389	21 40 16.9	39 11 44	0.502	0.226	0.012	-0.22	-0.45	cj
2200+420	22 02 43.3	42 16 39	3.593	5.570	0.301	-0.21	0.24	cj
2214+350	22 16 20.0	35 18 14	0.477	0.319	0.018	-0.06	-0.22	cj?
2229+695	22 30 36.5	69 46 28	1.365	0.591	0.031	0.80	-0.47	cj
2235+731	22 36 38.6	73 22 52	0.424	0.165	0.009	0.27	-0.53	cj
2238+410	22 41 07.2	41 20 11	0.677	0.226	0.012	0.12	-0.61	cj
2253+417	22 55 36.7	42 02 52	1.120	0.577	0.031	-0.18	-0.37	cj
2255+416	22 57 22.1	41 54 16	1.111	0.216	0.012	-0.41	-0.91	cj
2259+371	23 01 27.7	37 26 49	0.406	0.513	0.026	-0.30	0.13	cj
2309+454	23 11 47.4	45 43 56	0.597	0.401	0.020	0.53	-0.22	cj
2310+385	23 12 58.8	38 47 42	0.484	0.166	0.009	-0.28	-0.60	d
2319+444	23 22 20.4	44 45 42	0.366	0.282	0.015	0.14	-0.15	cj
2346+385	23 49 20.8	38 49 17	0.640	0.535	0.029	0.54	-0.10	cj
2351+456	23 54 21.7	45 53 04	1.145	1.223	0.062	-0.37	0.04	cj
2352+495	23 55 09.5	49 50 08	1.552	0.328	0.020	-0.32	-0.87	cso
2353+816	23 56 22.8	81 52 52	0.476 <sup>a</sup>	0.526	0.025	0.13 <sup>a</sup>	0.06	cj
2356+385	23 59 33.2	38 50 42	0.449	0.188	0.010	-0.28	-0.49	cj?
2356+390	23 58 59.9	39 22 28	0.371	0.414	0.020	-0.11	0.06	cj

<sup>a</sup> These spectral indices are calculated between 2.727 GHz and 5 GHz using data from Kuehr et al. (1981). <sup>b</sup> These identifications were made by Rossetti et al. (2005).